JOURNAL OF THE KOREAN ASTRONOMICAL SOCIETY
32: 17 ~ 39, 1999

DYNAMICAL EVOLUTION OF THE MULTI-MASS COMPONENT GLOBULAR CLUSTERS UNDER THE TIDAL INTERACTION WITH THE GALAXY

YOUNG KWANG KIM AND KAP SOO OH
Department of Astronomy and Space Science, Chungnam National University, Daejeon 305-764, Korea
E-mail: glory@astro2.chungnam.ac.kr, ksoh@astro6.chungnam.ac.kr
(Received Mar. 20, 1999; Accepted Apr. 16, 1999)

ABSTRACT

We investigate dynamical evolution of globular clusters with multi-mass component under the Galactic tidal field. We compare the results with our previous work which considered the cases of single-mass component in the globular clusters. We find the followings: 1) The general evolutions are similar to the cases of single-mass component. 2) There is no evidence for dependence on the orbital phase of the cluster as in the case of single-mass component. 3) The escape rate in multi-mass models is larger than that in the single-mass models. 4) The mass-function depends on radius more sensitively in anisotropic models than in isotropic models.

Key Words : celestial mechnics – stellar dynamics – clusters : globular – clusters : dynamics

I. INTRODUCTION

The dynamics of globular clusters has been studied for long time, since stars within a given cluster are coeval and have ages much larger than orbital period around the Galaxy. On these time scales, clusters with 10^{5-6} stars undergo significant internal evolution and the Galactic tide affects both the structure and evolution of the outer regions. It has been suggested that both internal processes and the tidal interaction with the Galaxy have determined not only the dynamical evolution of globular clusters (Ostriker, Spitzer, & Chevalier 1972; Spitzer & Chevalier 1973) but also their survival probability (Fall & Rees 1977; Aguilar, Hut, & Ostriker 1988; Ostriker, Binney, & Saha 1989). For these theoretical reasons, the analysis of the tidal evolution of globular clusters is very important. There have been several previous attempts to investigate the tidal evolution of globular clusters with limited scheme (Keenan & Innanen 1975; Spitzer & Shull 1975; Aguilar & White 1985; Seitzer 1985). More realistic approach has been adopted by Oh, Lin, & Aarseth (1992, hereafter Paper I) with single-mass component model. Their scheme utilizes Fokker-Planck approach as well as direct numerical integration of restricted three-body problem. Oh & Lin (1992, hereafter Paper II) presented the results which are obtained with this numerical method for various model parameters. After many observations of mass functions in globular clusters, especially after the Hubble Space Telescopes are launched (McClure et al. 1986 ; Richer et al. 1990 ; Capaccioli, Ortolani & Piotto 1991 ; Piotto 1991 ; Capaccioli, Piotto & Stiavelli 1993), multi-mass models are investigated. Lee, Fahlman & Richer (1991) examined the evolution of the mass function by integrating the Fokker-Plank equation with a steady Galactic tidal field. They showed that highly evolved clusters have a significant flattening of the mass function. Later Lee & Goodman (1995) calculate the evaporation rates for broad stellar mass function in tidally limited globular clusters and found that the fraction of the cluster mass lost per half-mass relaxation time is roughly constant and a significant fraction of the present-day Galactic cluster system will disappear within the next Hubble time. There are also direct N-body simulations for multi-mass models without tidal field (Giersz & Heggie 1996) and with tidal field (Giersz & Heggie 1997; Vesperini & Heggie 1997). Giersz & Heggie (1996) considered the effect of binaries and the circular orbit around the Galaxy of point mass. They found an increase in the mean stellar mass due to preferential escape of low mass stars and similar escape rates as Lee & Goodman (1995). But the effect of dormant binaries is turned out to be smaller in tidally limited systems than in isolated systems. Vesperini & Heggie (1997) investigated the evolution of multi-mass models with a power-law initial mass function of globular clusters driven by relaxation, stellar evolution and disk shocking, and including the effects of the tidal field of the Galaxy. Their results show that the global mass function becomes flatter depending on the fraction of the initial mass lost. And the mass function near the half-mass radius is least affected by mass segregation, but the mass function in the outer region becomes flatter than the initial mass function.

In this paper we consider the multi-mass component model of globular clusters. The Galactic tide and diffusion process are imposed. Some of the models are done for the eccentric orbits as well as circular orbits to consider the effect of time dependent tidal field. We divide the cluster into an inner region where two-body relaxation is important, and an outer region where the Galactic tide provides the most important dynamical perturbation as we did in Paper I. This boundary is referred as the critical radius.

For simplicity, we assume that the gravitational force inside the critical radius is dominated by the cluster. When a star crosses the critical radius into the inner

region, we map its position according to the predicted trajectory past pericenter to the exit phase from the inner region. During the excursion through this dense inner region, perturbations due to two-body relaxation are approximated self-consistently as diffusion through the three-dimensional velocity space. The diffusion coefficients are determined using a Fokker-Planck treatment for each mass component. From these diffusion coefficients, we compute the energy change during an orbital passage through the inner region. The effect of these perturbations are added to the velocity of the stars. Once a star moves outside the critical radius, the stellar density is too low to provide significant two-body relaxation effects. In this region, we integrate the equations of motion numerically, using a fourth-order force polynomial (Aarseth 1985) and include both the cluster potential and the Galactic tidal field. We use the conservative criterion (ten times of initial theoretical tidal radius) to remove the escapers because not only there is a uncertainty in tidal radius (Allen & Richstone 1988 ; Ross, Mennim & Heggie 1997), but also we want to examine the mass function beyond the tidal radius.

Although time dependent tide and logarithmic potential for the Galaxy are adopted, several factors have been omitted including the disk shocking. For both inner and outer regions, we assume the cluster potential to be spherically symmetric and constant in time. The stellar distribution in the outermost regions of the cluster is unlikely to be spherically symmetric; however, most of the mass remains well inside this region. Although there is mass loss from the cluster as stars escape, this will have negligible effects on the cluster potential over a Galactic orbital time scale, especially for the case of low escape rate. Also the influence of primordial binaries are neglected. They don't seem to have an important role in the tidal stripping process (Giersz & Heggie 1997).

The orbital kinematics, equations of motion, mass function, distribution function, calculation of diffusion coefficients and velocity perturbations are described in Section II. In Section III, the cluster models, potential of the cluster and the Galaxy are described. Initial parameters of the models are discussed in Section IV. We present results of the simulations and discuss those result in Section V.

II. ORBITAL KINEMATICS

(a) Equations of Motion

The size of globular clusters is typically two orders of magnitude smaller than their distance from the Galactic center. The stellar velocity dispersion of the clusters is also about an order of magnitude smaller than the characteristic orbital velocity around the Galaxy. If the evolution of the cluster stars is computed in an inertial frame with respect to the Galactic center, the accumulated numerical truncation errors would significantly jeopardize the accuracy of the results. We find it advantageous to carry out the numerical computation in a comoving frame such that the guiding center of the frame is centered on the cluster core. Thus the frame corotates with the instantaneous orbital frequency where the azimuthal phase is defined with respect to the direction of the Galactic center. Consequently, this rotation rate of the comoving frame is not constant for the eccentric orbit.

We use the equations of motion for individual stars and the guiding center in the Appendix of Paper I in our simulations.

(b) Mass Function

The observation of the initial mass function in globular clusters is not easy because high mass stars turned into white dwarf which is difficult to see. And dynamical evolution of globular clusters lead the significant amount of evaporation during their life time (Lee & Goodman 1995). Therefore it is difficult to get the mass function from the present day observations. However Salpeter type power law can be adopted. This power-law mass function is defined by $dN = C_o m^{-x} d(\log m)$, if N is the number of stars in a mass (m) bin. There is no particular reason to use a power-law mass function, but it is a simple form and the range of masses of interest sufficiently small that the exact form does not matter very much. Gunn & Griffin (1979) explored the power index for the mass function of M3. And we adopt the index of 1.3 among their values.

In the models we use, the masses (m) are binned in five intervals of 0.179 in the range of $\log m$ = -0.06 $\sim$ -0.950. If M is the total mass in a bin in $\log m$, and the upper and lower limits of the bin masses are m_j and m_{j+1} respectively, then the mass M_j in the bins are

$$M_j = \int_{m_j}^{m_{j+1}} C_o m^{-x} d(\log m)$$
$$= \frac{C_o}{(1-x)\ln 10} m_{j+1}^{1-x} \{1 - (\frac{m_j}{m_{j+1}})^{1-x}\} \qquad (m_{j+1} > m_j) \qquad (1)$$

where C_o is the constant which is determined by a given total mass. Five mass classes are adopted from the average mass in each bin. So the maximum mass ratio between high and low mass stars is m_{max}/m_{min} = 5.153. The mass range, average mass, total mass ratio (M_j/M_t) and relative numbers (N_j/N_t) in each bin are listed in Table 1.

(c) Distribution Functions

In order to determine the cluster potential and evaluate diffusion coefficients, we need to specify a phase space distribution function for the stars. King (1966) adopted a simple distribution function for isotropic velocity dispersion and the distribution function for anisotropic velocity dispersion (Gunn & Griffin 1979)

Table 1. Mass range, bin mass, relative total mass and relative numbers

bin	mass range(log$m$)	average mass ($M_\odot$)	M_j/M_t	N_j/N_t
1	-0.060 ~ -0.239	0.7245	0.154	0.0527
2	-0.239 ~ -0.416	0.4809	0.174	0.0898
3	-0.416 ~ -0.594	0.3192	0.197	0.1530
4	-0.594 ~ -0.772	0.2119	0.223	0.2606
5	-0.772 ~ -0.950	0.1406	0.252	0.4400

in a mass bin j is

$$f_j(E,J) = C_j \exp(-A_j J^2/2r_a^2)[\exp(-A_j E) - 1], \quad (2)$$

where E and J are the local orbital energy and angular momentum of the stars respectively, C_j is the normalization constant, A_j is the constant for dimensionless in exponential and r_a is the anisotropy radius. Then the number distribution function is

$$g_j(E,J) = f_j(E,J)/m_j. \quad (3)$$

And these distribution functions can be written in (r,v) space as

$$f_j(r,v) = C_j \exp(-\beta m_j v_t^2 r^2/2r_a^2) \times \quad (4)$$
$$[\exp\{-\beta(0.5 m_j v^2 + m_j \psi(r))\} - 1],$$

$$g_j(r,v) = f_j(r,v)/m_j, \quad (5)$$

where $\beta = A_j/m_j$, v_t is the transverse velocity of the star and ψ is the potential. If we measure velocities and radii in terms of the central velocity dispersion and core radius, respectively, and scale the potential by the square of central velocity dispersion, then equations (2), (3), (4) and (5) can be converted into dimensionless forms. After the density is obtained by integrating the above distribution function in velocity space, we find the potential by solving the Poisson equation (Gunn & Griffin 1979).

(d) Diffusion Coefficients

Two-body encounters do not introduce significant changes in the stellar orbital angular momentum because the symmetry in the distribution about the trajectories leads to cancellation of the perturbations in transverse directions. This symmetry is preserved on all but the largest scales in the clusters. However, during one orbital period, Δt, two-body interactions induce energy changes for one mass component $\epsilon_j^2 = \epsilon_{1,j}^2 + \epsilon_{2,j}^2$ (Spitzer & Shapiro 1972), with

$$\epsilon_{1,j} = 2\int_{r_p}^{r_{ap}} < \Delta E_j > \frac{dr}{v_r}, \quad (6)$$

$$\epsilon_{2,j}^2 = 2\int_{r_p}^{r_{ap}} < (\Delta E_j)^2 > \frac{dr}{v_r}, \quad (7)$$

where r_p and r_{ap} are pericenter and apocenter distances, and v_r is the radial velocity. The change of energy, ΔE_j, in a single encounter is given by equation (5-24) of Spitzer (1962) as

$$\Delta E_j = v\Delta v_{\|} + \frac{1}{2}(\Delta v_{\|})^2 + \frac{1}{2}(\Delta v_{\perp})^2, \quad (8)$$

where v is the velocity, and $\Delta v_{\|}$ and $\Delta v_{\perp}$ are the collisionally induced changes of v in the directions parallel and perpendicular, respectively, to the original trajectory. Because of the nearly symmetric mass distribution, the mean value of ΔE_j is of the order of $< (\Delta v_{\|})^2 >$. If only dominant terms are considered in equation (8), the mean value of $(\Delta E_j)^2$ becomes of the order of $v^2 < (\Delta v_{\|})^2 >$. Thus as in Paper I the ratio is

$$\frac{\epsilon_{1,j}}{\epsilon_{2,j}} \sim \frac{< \Delta E_j > \Delta t}{\sqrt{< (\Delta E_j)^2 > \Delta t}} \sim \frac{\sqrt{< (\Delta v_{\|})^2 > \Delta t}}{v} \ll 1. \quad (9)$$

We can therefore neglect the $\epsilon_{1,j}$ contribution to the energy change in computing the tidal evolution of the outer regions of the cluster. In general, however, contribution due to $\epsilon_{1,j}$ may lead to core collapse and therefore must be taken into account in computing the internal evolution of globular clusters.

As in Paper I, we average the distribution function over a range of angular momentum and the energy perturbation for a given mass class (j) is the sum of perturbations from all the mass classes (i's). Following the equation (A4b) of Shapiro and Marchant (1978), the energy perturbation is

$$\epsilon_{2,j}^2(E,J) = \sum_{i=1}^{5} \frac{\alpha_{ji}}{6} \times$$
$$\left\{ \int_{\xi_p}^{\xi_{ap}} \frac{u^2}{u_\xi} d\xi \left[\int_E^0 \bar{g}_j(E')dE' + \int_{-W(\xi)}^{E} \bar{g}_j(E') z_\xi^3 dE' \right] \right\}, \quad (10)$$

where $\alpha_{ji} = 128\pi^2 m_i^2 \ln\Lambda_{ji}$, $\Lambda_{ji} = 2\gamma M_i/(m_j + m_i)$, $\gamma = 0.4$, M_i is the total mass in mass class i, $z_\xi \equiv \{[E' + W(\xi)]/[E + W(\xi)]\}^{1/2}$, $u = [2E + 2W(\xi)]^{1/2}$ is the total velocity, $u_\xi = [2E + 2W(\xi) - J^2/\xi^2]^{1/2}$, and $W(\xi)$ is the dimensionless potential energy at dimensionless radius ξ. In our calculations, we take the upper limit of integration to be the critical radius. To speed up the numerical calculation these diffusion coefficients

are tabulated for an appropriate range of energy and angular momentum for each mass class, and these tabulated values are interpolated in the simulation. This diffusion coefficient in lowest mass class is about 10% larger than in highest mass class.

(e) Velocity Perturbations

To determine the velocity perturbations in mass class j during one orbital period, Δt, we find from equations (7) and (8)

$$\epsilon_{2,j}^2 \equiv 2 \int_{r_p}^{r_{ap}} < (\Delta E_j)^2 > \frac{dr}{v_r}$$
$$=< (\Delta E_j)^2 > \Delta t = v^2 < (\Delta v_{||})^2 > \Delta t. \quad (11)$$

Following the prescription by Spitzer and Thuan (1972), we introduce perturbations Δv_r and Δv_t to the radial and transverse velocities such that

$$\Delta v_r = X \left\{ < (\Delta v_{||})^2 > \Delta t \right\}^{1/2} \frac{v_r}{v} = X \frac{\epsilon_2 v_r}{v^2}, \quad (12)$$

$$\Delta v_t = X \left\{ < (\Delta v_{||})^2 > \Delta t \right\}^{1/2} \frac{v_t}{v} = X \frac{\epsilon_2 v_t}{v^2}, \quad (13)$$

where X in equations (12) and (13) denotes random numbers from a Gaussian distribution with zero mean and unit variance.

The perturbations in the orbital angular momentum of the stars is neglected, i. e. contribution from ΔJ is ignored. This approximation is adequate for the representative halo stars which we are studying because they primarily interact with stars in cluster core where the density is relatively large. When these stars enter the core region, they are on nearly parabolic orbits such that most of the encounters may be regarded as distant encounters. In the cluster core, the background stellar density is essentially homogeneous and velocity distribution approximately isotropic for all encounters including the encounters with impact parameters comparable to the core radius. Due to the lack of any effective torque, $|\Delta v_\perp / \Delta v_{||}| << 1$. For the analysis of interaction between stars in the cluster core, the contribution from $\Delta v_\perp$ must be taken into account.

III. CLUSTER MODELS

Two particular models of isotropic and anisotropic velocity dispersions are used to determine the cluster potential and phase space distribution function. We adopt the units $G = 1$, central density $\rho_o = 1$ and core radius $r_c = 1$. This gives the central velocity dispersion of the cluster as $v_o = 2\sqrt{\pi}/3$.

(a) Internal Kinematic Models of the Cluster

In all our computations, we use two sets of cluster models: an isotropic model and an anisotropic model.

The isotropic model is generated from the King distribution function with a central potential $W_0 = 10.56$. The outer cutoff radius where the distribution function [eq. (2)] vanishes is about 56 r_c. The half-mass radius in this isotropic case is 9.91 r_c. When these values are appropriately scaled, the characteristic dynamical time scale, τ_c, is $2.32 \times 10^6 (R_c^3/M_5)^{1/2}$ yrs, where R_c is the core radius in units of pc and M_5 is the cluster mass in units of $10^5 M_\odot$. The anisotropic model is generated from the King-Michie distribution function with $W_0 = 9.385$ and $r_a = 5.4$. The outer cutoff radius is about 196 r_c. The half-mass radius in this anisotropic case is 14.13 r_c. The characteristic dynamical time scale is $3.95 \times 10^6 (R_c^3/M_5)^{1/2}$ yrs. The structure of many globular clusters can be approximated by these models (Peterson & King 1975; Illingworth & Illingworth 1976; Webbink 1985).

We choose the critical radius to be 10 r_c and 40 r_c in the isotropic and anisotropic cases, respectively. Interior to these radii, the Galactic tidal force contributes less than 0.8% of the gravitational force. The mass inside the critical radius is 50.4% of total mass for the isotropic case and 80.7% for the anisotropic case. We generate an initial distribution of 10000 stars between the critical radius and cutoff radius. If the total mass of the globular cluster is $1.126 \times 10^5 M_\odot$ and the stellar distribution is extrapolated to the cluster core, these number in the outer regions correspond to a total number of 2.582×10^5 stars for the isotropic case and 1.134×10^5 stars for the anisotropic case. And the numbers of particles(n_j) in the simulations and the corresponding real number of stars(n'_j) in isotropic and anisotropic cases are listed in Table 2.

(b) Approximations of the Cluster's Potential and Trajectory

We now introduce several simple functions to approximate the acceleration and potential of the cluster which are assumed to be fixed during the evolution due to a small number of escaping stars. Outside the critical radius, where the orbits are integrated directly, we approximate the cluster acceleration, g, by

$$g = \begin{cases} \frac{a_i}{\xi^2 + b_i} + c_i, & \xi \leq \text{cutoff radius}; \\ \frac{d_i}{\xi^2}, & \xi > \text{cutoff radius}, \end{cases} \quad (14)$$

Table 2. Number of particles and corresponding number of stars

bin	isotropic		anisotropic	
	n_j	$n'_j(10^4)$	n_j	$n'_j(10^4)$
1	147	0.38	43	0.05
2	638	1.65	321	0.36
3	1451	3.75	1052	1.19
4	2773	7.16	2660	3.02
5	4991	12.9	5924	6.72

where a_i, b_i, c_i and d_i are constants, $i = 1$ for the isotropic case, $i = 2$ for the anisotropic case, and their values are given in Table 3. These approximations lead to the relative error less than 1.5%, which is adequate for the present purpose.

After integration the equation (14) we get the approximate form of the potential $W(\xi)$

$$W(\xi) = \begin{cases} a_i \tan^{-1}(b_i \xi) + c_i \xi^{m_i} + d_i, & \xi \leq \text{cutoff radius;} \\ 0, & \xi > \text{cutoff radius,} \end{cases} \quad (15)$$

where a_i, b_i, c_i, d_i and m_i are constants, $i = 3$ for the isotropic case, $i = 4$ for the anisotropic case, and their values are also given in Table 3.

Inside the critical radius, orbital energy and angular momentum are conserved in the absence of two-body relaxation processes. Thus, the stars leave the critical radius with the same speed as they enter but the direction of radial motion is changed. Instead of detailed computation, an orbit is easily determined when the change in the trajectory angle, $\Delta\theta$, due to pericenter passage is specified. For a star with energy, E, and angular momentum, J,

$$\Delta\theta(E, J) = 2 \int_{\xi_p}^{\xi_{crit}} \frac{J}{\xi^2} \frac{d\xi}{u_\xi}$$

$$= 2 \int_{\xi_p}^{\xi_{crit}} \frac{J d\xi}{\xi^2 \sqrt{2[E + W(\xi)] - J^2/\xi^2}}, \quad (16)$$

where ξ_{crit} is the critical radius. To speed up the numerical calculation the angle changes are tabulated for an appropriate range of energy and angular momentum as in the case of the diffusion coefficient, and these tabulated values are interpolated in the simulation for the trajectory.

(c) Initial Cluster Size and Orbital Parameters

We consider two types of orbits. In one case, the cluster is in a circular orbit around the Galaxy. The length scale is set such that the initial cutoff radius (56 and 196 r_c in the isotropic and anisotropic cases respectively) to be the theoretical tidal radius of the cluster. In the second type of orbits, the cluster is in an orbit with eccentricity $e = 0.5$. Here, we set the initial cutoff radius to be that of the theoretical tidal radius at perigalacticon. Assuming a logarithmic potential for the Galaxy and following King's (King 1962) method, the tidal radius is give in the eq. (23) in Paper I.

Although this definition of tidal radius is uncertain and controversial (Innanen 1979; Allen & Richstone 1988 ; Ross, Mennim & Heggie 1997), it is reasonably accurate because the cluster may approach equilibrium after a few Galactic orbits. Because of these uncertainties in the tidal radius, we remove escaping stars outside 10 times the initial cutoff radius, which is at least several times larger than the tidal radius at apogalacticon.

The Galactic mass is set to zero initially and is increased to its full value over 1/20 of a cluster crossing time such that the initial perturbations due to the Galactic tidal force are reduced.

(d) Limitation of Method

As in Paper I, the numerical scheme we outlined above is explicitly designed for the simulation of tidal interaction between globular clusters and the Galaxy. It is not a general purpose scheme and should be used with caution. For example, we adopted the cluster with full mass segregation and neglected the further secular evolution in dynamical friction process and therefore it is inappropriate to use the scheme for the simulation of internal dynamics of the cluster. The core collapse phenomenon cannot be simulated by this scheme. Also, we neglected secular changes in the cluster's mass distribution and potential. Therefore, it is inadequate for the simulation of tidal interaction between the Galaxy and marginally bound stellar systems, such as dwarf galaxies and open clusters where a substantial mass loss may be expected.

IV. MODEL PARAMETERS

We computed a large number of models to get the dependence on the influence of the range of the Galactic tidal fields and two-body relaxation strength. Only several illustrative models will be presented here.

We consider only spherically symmetric Galactic potentials in which the clusters' energy and angular momentum are conserved along their Galactic orbit. In all the cases below, we performed computations for a logarithmic spherically symmetric Galactic potential.

The strength of the Galactic tidal effect also depends on cluster's orbital eccentricity on which very little observational information is available. Statistical analyses of globular cluster kinematics (Frenk & White 1980) suggest large spread in clusters' orbital eccentricity. In this study, we examine a circular orbit and an eccentric orbit with $e = 0.5$. These two types of orbit are described in detail in §3.3 in Paper I.

The parameters of several illustrative models are summarized in Table 4. The first column shows the model names. Models I2 through I6 have an isotropic while Models A2 through A9 have anisotropic velocity distributions. The total number of stars ($\bar{N}$) gotten from the averaged mass of each mass class is given in Column 2 in units of $10^5 M_\odot$. Column 3 lists the ratio of the mass of the Galaxy (M_G) to that of a cluster (M_c) in units of $10^6 M_\odot$, where M_G refers to the Galactic mass inside the semi-major axis of the cluster. Column 4 gives the radius of a circular orbit, or the semi-major axis (a) of an eccentric orbit, in units of 10^4 core radii. The eccentricity (e), defined by equation (24) of Paper I, is given in Column 5. We define an orbital period, τ_o, as the time taken for one complete circular orbit or twice the time taken from apogalacticon to perigalac-

Table 3. Numerical values of constants

constant	i = 1	i = 2	i = 3	i = 4
a_i	31.711365	71.244218	-5.502078	-2.597515
b_i	29.256796	3.858764×10^{2}	9.27006×10^{-2}	5.09068×10^{-2}
c_i	-7.906872×10^{-3}	1.733153×10^{-5}	4.08356×10^{-4}	-1.24127×10^{-5}
d_i	78.114250	71.201518	7.590093	3.822718
m_i	...	...	0.5	1.0

Table 4. Model Parameters

Model (1)	$N(10^5)$ (2)	$M_G/M_c(10^6)$ (3)	a (4)	e (5)	τ_o/τ_c (6)	τ_r/τ_c (7)	τ_r/τ_o (8)	Comments (9)
I2	3	...	...	...	...	...	...	diffusion
I3	3	2.000	0.8889	0.0	75.49	2271.72	30.09	tide
I4	3	2.000	0.8889	0.0	75.49	2271.72	30.09	tide, diffusion
I5	3	0.288	0.8889	0.5	142.81	2271.72	15.91	tide
I6	3	0.288	0.8889	0.5	142.81	2271.72	15.91	tide, diffusion
A2	30	...	...	...	...	18980.3	...	diffusion
A4	30	1.000	2.4694	0.0	290.31	18980.3	65.38	tide
A6	3	2.000	3.1113	0.0	290.31	2271.72	7.83	tide, diffusion
A7	30	0.144	2.4694	0.5	553.49	18980.3	34.29	tide
A9	9	0.480	3.6887	0.5	553.49	6229.93	11.26	tide, diffusion

ticon for an eccentric orbit. The crossing time, τ_c, is defined as the time required for a star moving with the rms velocity to traverse the half-mass radius. The ratio of an orbital period to the crossing time is given in Column 6. The ratio of the half-mass relaxation time, τ_r, to the crossing time, defined by $N/\{26 \log (0.4N)\}$ (Spitzer & Hart 1971), where N is the total number of stars in the cluster replaced by $\bar{N}$, is given in Column 7. Column 8 contains the ratio of the relaxation time to an orbital period. Finally, Column 9 summarizes the properties of each model.

V. RESULTS AND DISCUSSION

We study a series of model parameters which allows an exploration of the parameter dependence. The main issues we wish to examine are the dependence of tidal evolution on: 1) the internal velocity distribution of the stars, 2) the strength of the Galactic tide, 3) the rate of two-body relaxation, 4) the escape rates, and 5) mass function. Numerical simulations generate large quantities of data. The most useful information is contained in the spatial density ρ, surface density σ, the energy and angular momentum distributions, the ratio of transverse velocity v_t and radial velocity v_r, and the fraction of stars with retrograde orbits N_{ret} with respect to the orbital motion of the cluster. The correlation between energy and angular momentum indicates the eccentricity of stellar orbits in the cluster. In our analysis, the energy of each star is computed using the potential of an isolated cluster which is set to zero at infinity, while the potential of the Galaxy is neglected. In order to preserve statistical significance, we also set the spatial density and surface density at a given radial bin to zero if the number of stars in this bin is less than three. The most important goal of multi-mass model is to compare results with those of single-mass model and the evolution of mass function.

We simulate the isolated system over 50 Galactic orbits to test the numerical stability of the code. And the results are very stable in spatial density, in surface density and in energy-angular momentum distributions. Although few stars migrate slightly beyond the initial cutoff radius, resulting in a small expansion of the cluster radius due to initial random choice of the velocities.

(a) Spatial Density

Spatial density plots for several models are shown in Figure 1. There are more diffusion effect in single-mass models than in multi-mass models (Model I2 and A2 in Paper I), especially in anisotropic model. The limiting radius in simulations with eccentric orbits in Model I5 and A7 are more extended than those of Model I3 and A4 due to relatively smaller tidal force, Coriolis force and centrifugal force. The case of the tide and diffusion process are also given in Figure 1. The density decreases homologously as in the case of single-mass case (Model I6, A9 in Paper II). The profile in these multi-mass cases are very similar to those in single-mass cases. To check the time dependence of tidal force the

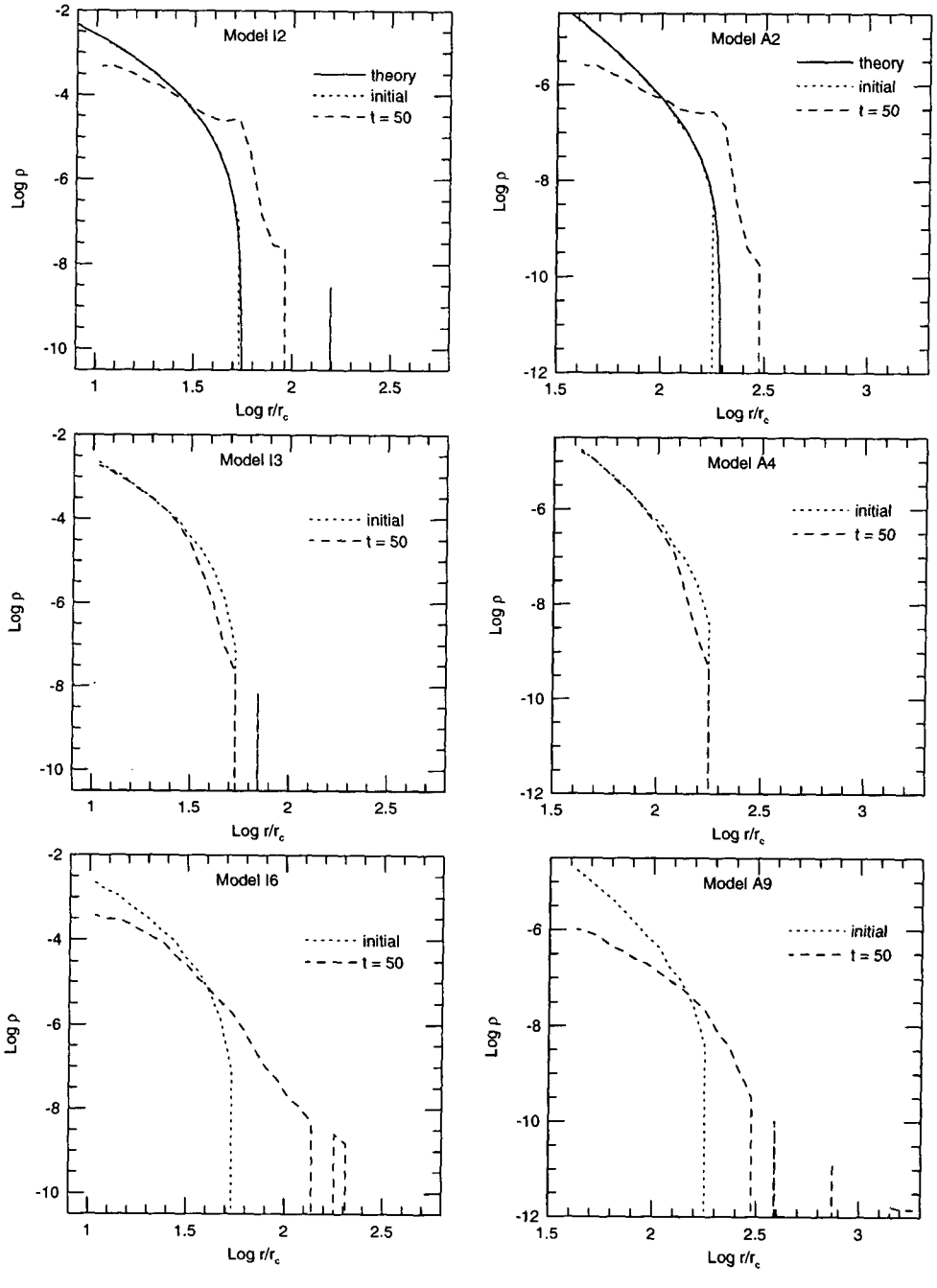

Fig. 1.— Density plots at initial and after 50 orbital time.

results from models with orbital eccentricity of 0.5 are in Figure 2 in several orbital phases. And there is not much phase dependent.

(b) Surface Density

Surface density plots for various models show the similar trend to the spatial density plots. And the plots of two models (Model I6 and A9) are in Figure 3. They also show no orbital phase dependence.

(c) Energy and Angular Momentum

We compare the plots of energy and angular momentum in multi-mass models with the results in single-mass models. Most of the models do not show much differences, and one of them are shown in Figure 4a. The plots of single-mass case are also shown for comparison. In this isotropic case, there is a broad spread of angular momentum for any given energy as expected. However significant differences are found in models A2, A4 and A9. And their results are shown in Figures 4b, 4c and 4d respectively. The concentrated part of upper left in Figure 4a at $t = 50\tau_o$ is the stars which do not no longer enter inside the critical radius because their orbital eccentricities are small after the tidal evolution. The sharp boundary in upper part of each figure is due to the maximum angular momentum for given energy, i.e. a circular orbit. The anisotropic models in multi-mass cases have more stars than those in single-mass cases near this sharp boundary. This is because the distribution of each mass component is different due to mass segregation, which can lead low mass stars to have small eccentricities. The sharp edges lower left at $t = 50\tau_o$ in Model A2 (Fig. 4b ; diffusion only case) are artificial and due to the same effect which causes a break in the density profile, i.e. the inconsistency between the stellar distribution function of the tidally truncated initial King-Michie models and that of isolated evolved models. Once again, when the Galactic tidal effect is included, these edges will vanish.

The evaporated stars migrate into the high-energy regions of phase space. This is because the main effect of two-body relaxation is a diffusion in energy. Stars diffuse to large radii as a result of energy gain rather than angular momentum gain. Consequently their orbits become more eccentric. Since two-body relaxation occurs near the center where the density has a maximum, orbits with large orbital semi-major axis would stop evolving unless they have a sufficiently large eccentricity to allow them to return to the cluster core. There are fewer stars in lower energy regions for most of the models after 50 orbital time. The general pattern of angular momentum and energy evolutions are very similar to the evolution in single-mass cases in Paper II.

(d) The Ratio of Transverse and Radial Velocity Dispersions

For the isotropic cases, there is no significant evolution on the time scale of 50 Galactic orbits in tide only model (Model I3), although mean of transverse components are increased in Model I4 in which the tide and diffusion are considered. For the anisotropic models, the initial magnitude and dispersion of v_t is much smaller than those of v_r in the outer regions of the cluster. Galactic tidal torque induces angular momentum to the stellar orbit about the cluster center which increases the magnitude and dispersion of v_t. Since the clusters' gravity dominates near the cluster core, stars in the outer regions of the cluster are more strongly perturbed. In contrast to the initial theoretical velocity ratio distributions (the solid lines), the outer regions of the cluster become increasingly isotropized with time. The general time evolution of velocity distribution in multi-mass models are similar to those in single-mass models in Paper II except the models whose orbits are eccentric around the Galaxy. In these models low mass stars occupy the higher angular momentum region where the tangential velocity is big. So the net number of these stars is higher than that of single mass stars. Two of these models are plotted in Figure 5 for illustrations. We also note that for the eccentric models, there is no evidence for dependence on the orbital phase of the cluster.

(e) The Fraction of Stars with Retrograde Orbits

Although the diffusion process is equally efficient for direct and retrograde orbits, the external tide differentially affects the stability of these orbit. Near the theoretical tidal radius the direct orbital motion and its prolonged action induces a considerable exchange of energy and angular momentum between the cluster's Galactic orbit and the stellar orbits in the cluster. Consequently, stars with direct orbits are most easily tidally removed from the cluster. In contrast, stars with retrograde motions have brief and frequent inferior conjunction such that the energy and angular momentum exchange rate due to the Galactic tidal torque is averaged to much smaller values. These orbits are much more stable. These features in multi-mass models are very similar to those in single-mass models and two of representative models (I6 and A9) are given in Figure 6. In theses models the escapers are consisted of near same amount of direct and retrograde orbit stars after first orbital period because initial velocity distribution of both kinds of stars are random, so some of them can go further than the cutoff radius. Then those stars with nearly same ratio of direct and retrograde orbits can escape easily under the tide and diffusion.

(f) The Escape Rates

We may estimate the evaporation rate of stars from a cluster by assuming that a Maxwellian distribution

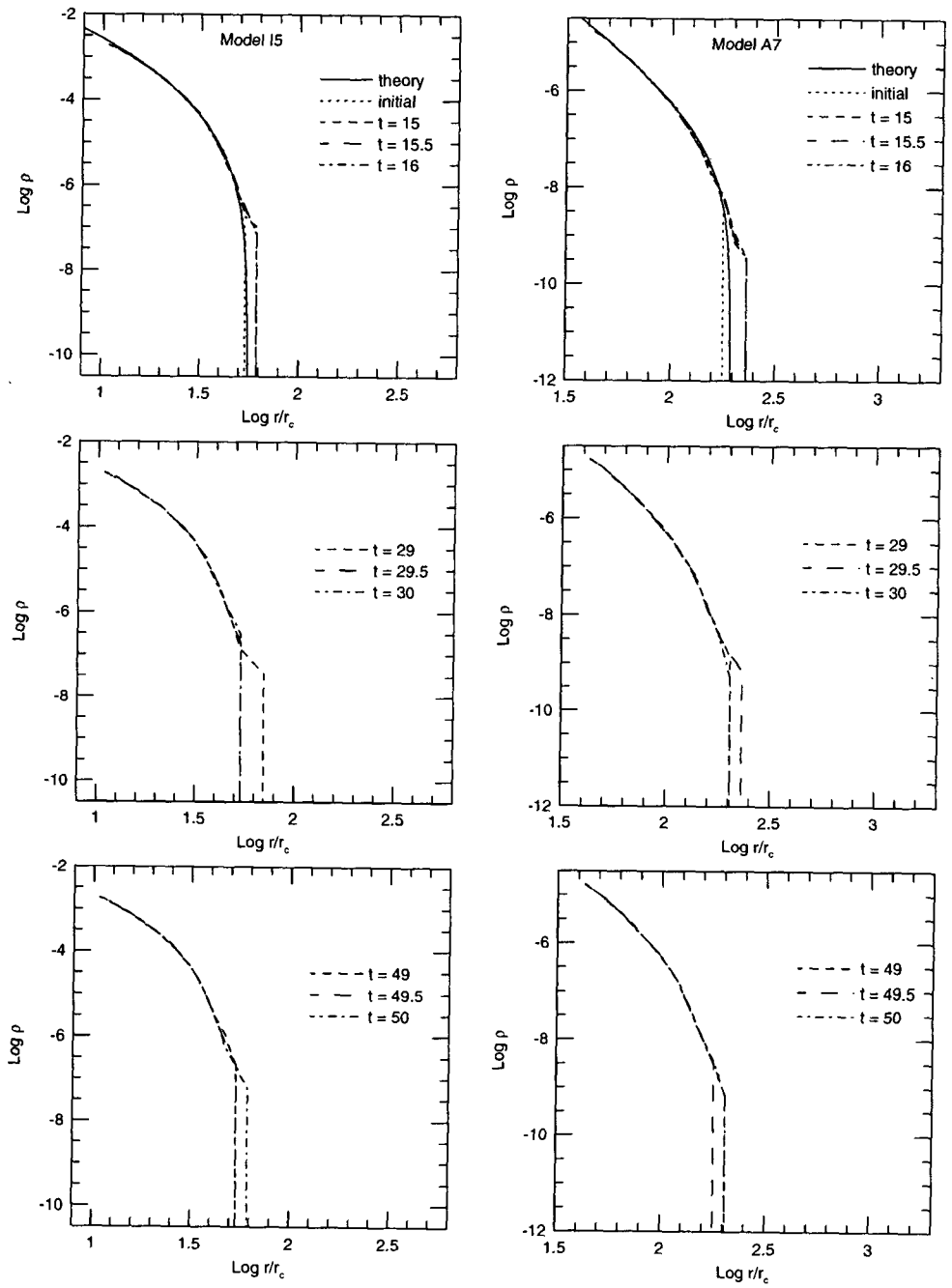

Fig. 2.— Density plot at different orbital times for isotropic (Model I5) and anisotropic (Model A7) velocity dispersions.

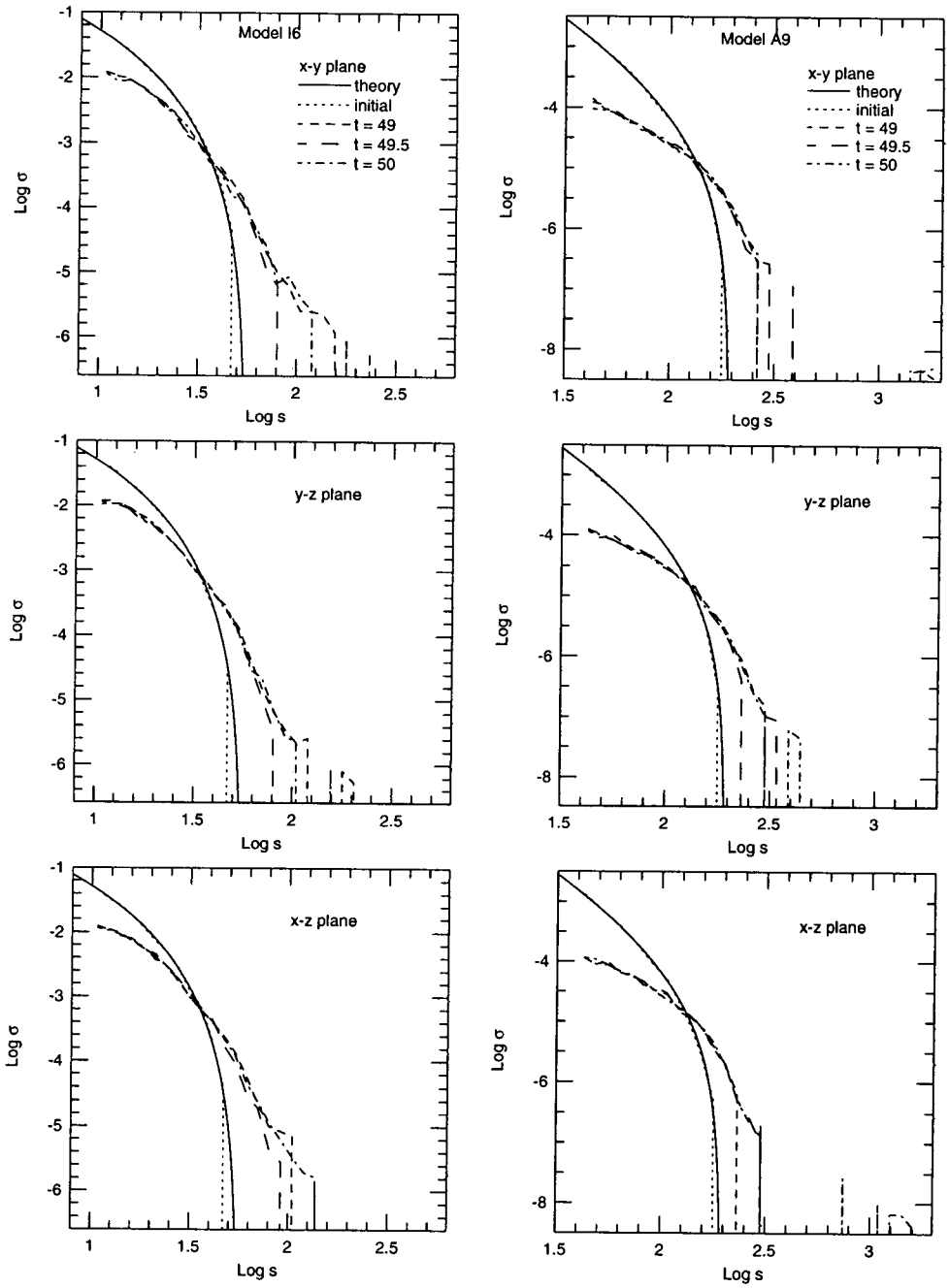

Fig. 3.— Surface density plot at different orbital times.

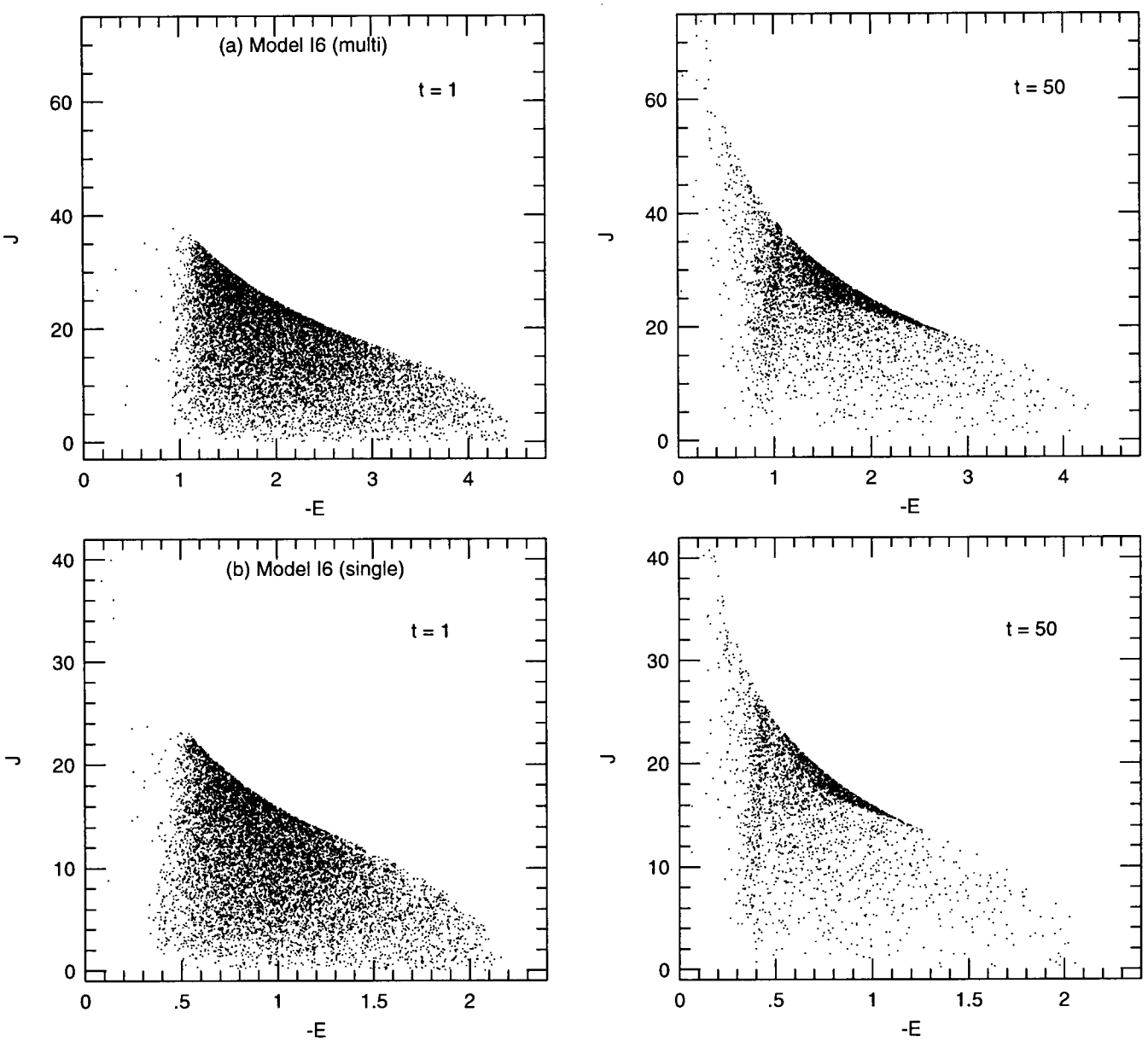

Fig. 4(a).— Energy and angular momentum of Model I6 in multi-mass case and single-mass case.

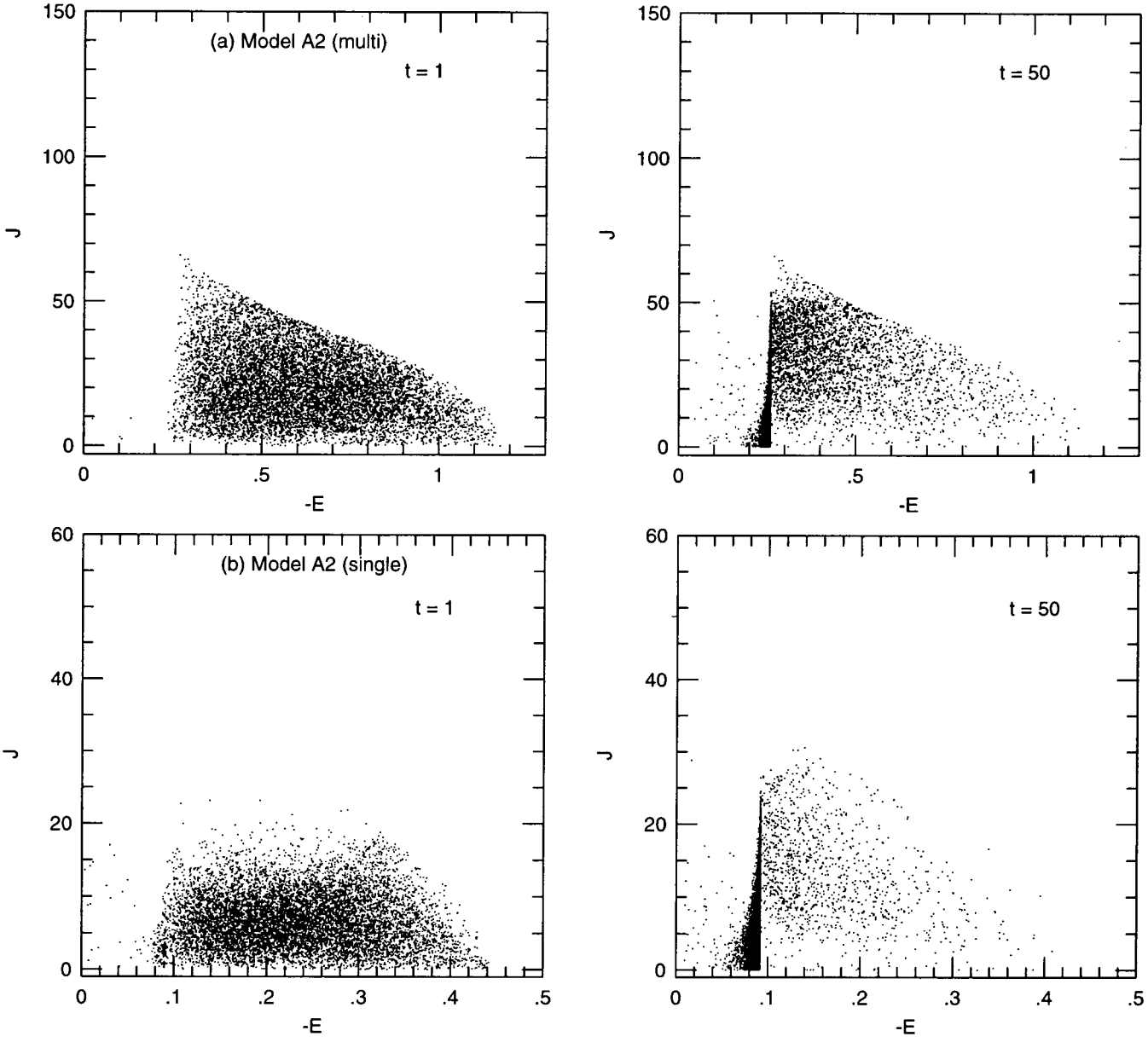

Fig. 4(b).— Energy and angular momentum of Model A2 in multi-mass case and single-mass case.

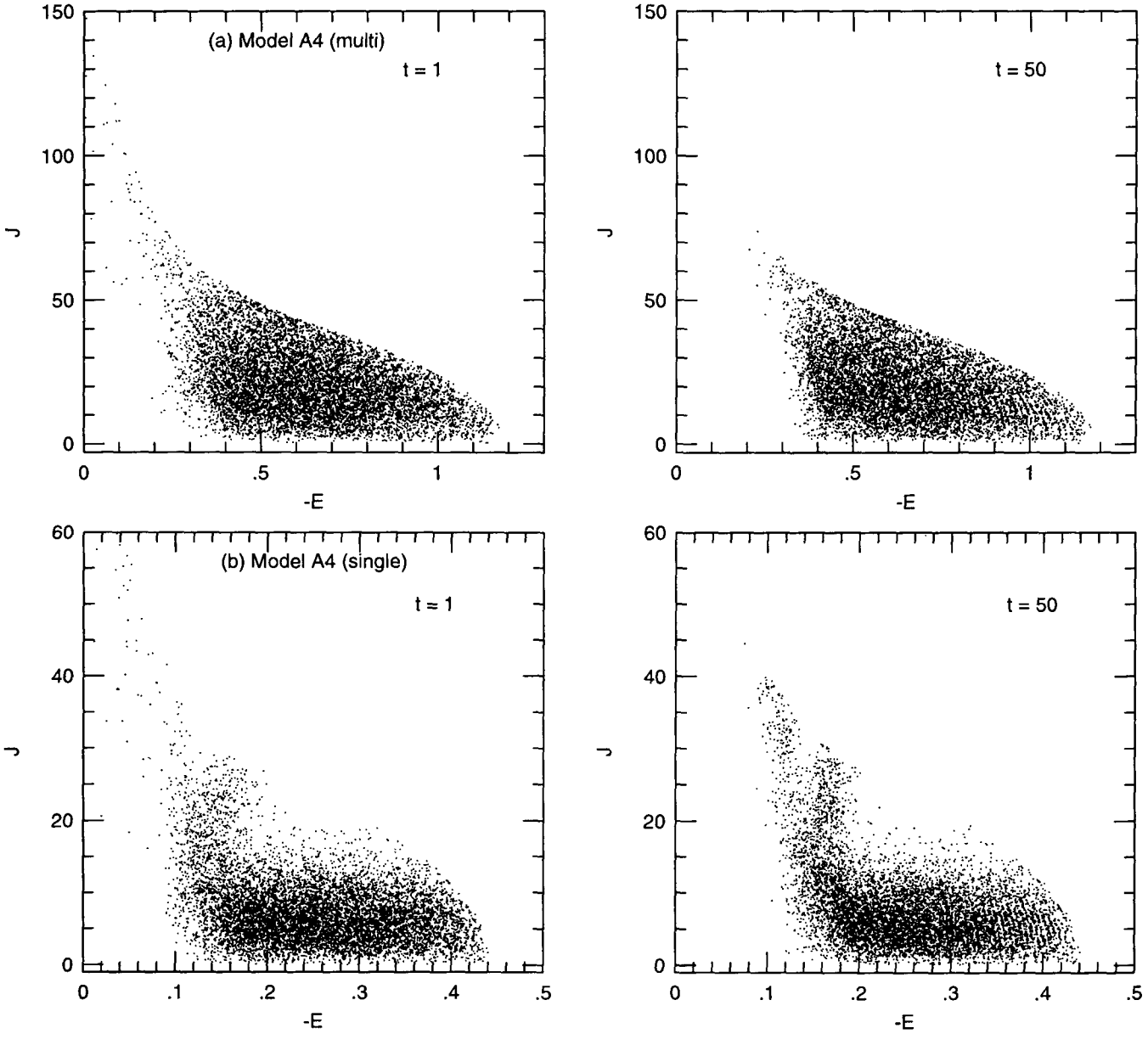

Fig. 4(c).— Energy and angular momentum of Model A4 in multi-mass case and single-mass case.

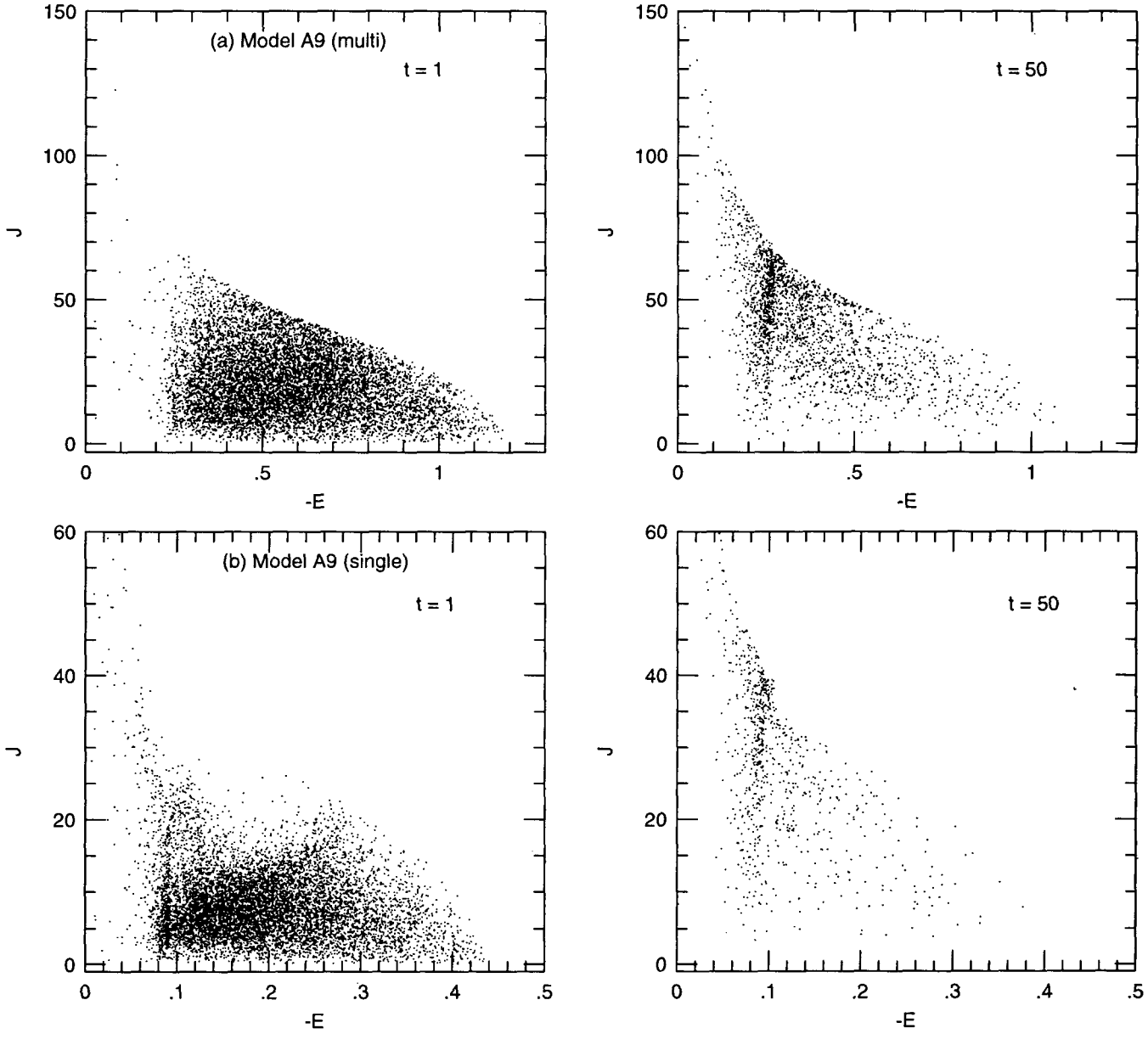

Fig. 4(d).— Energy and angular momentum of Model A9 in multi-mass case and single-mass case.

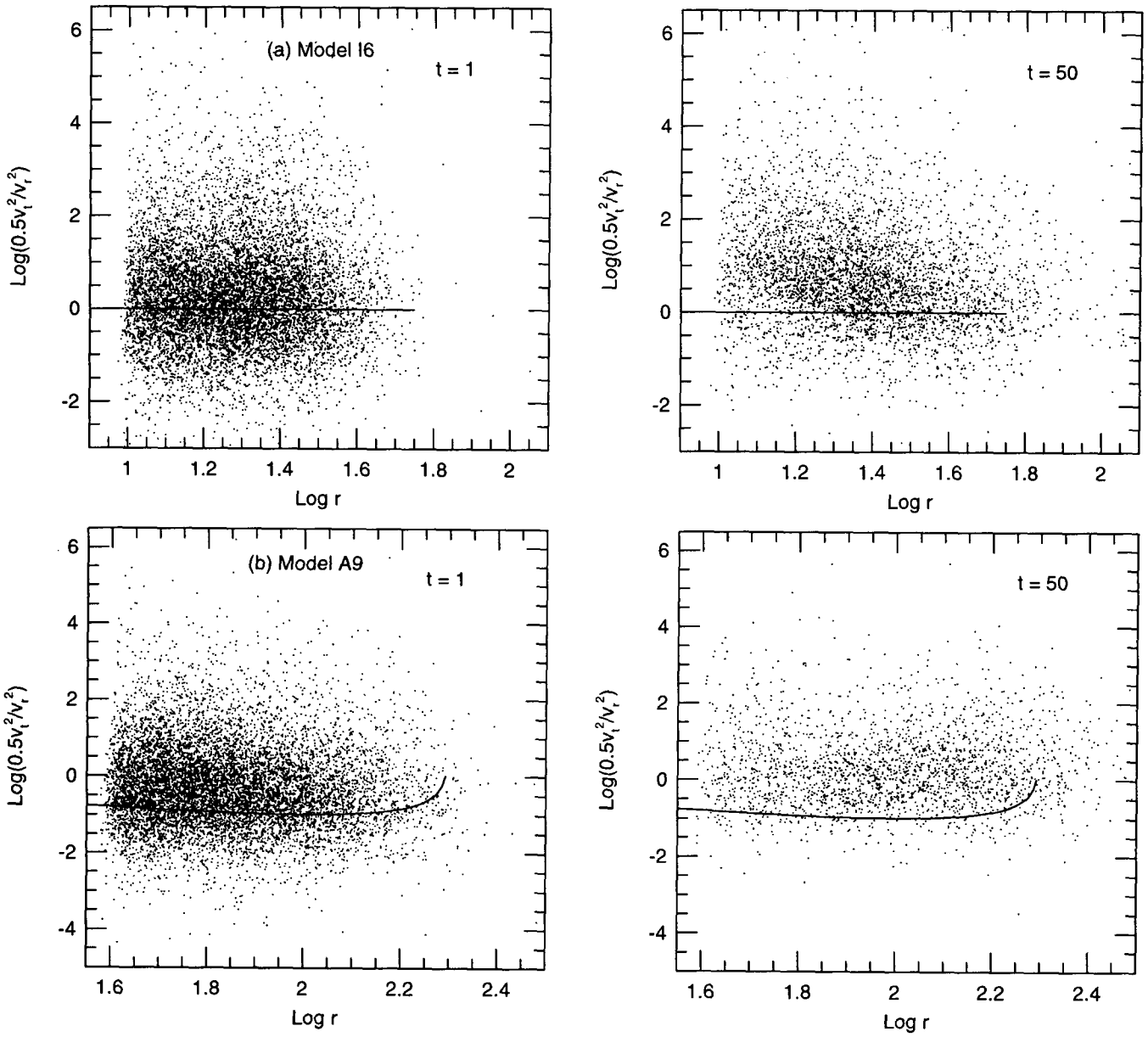

Fig. 5.— The ratio of transverse and radial velocities.

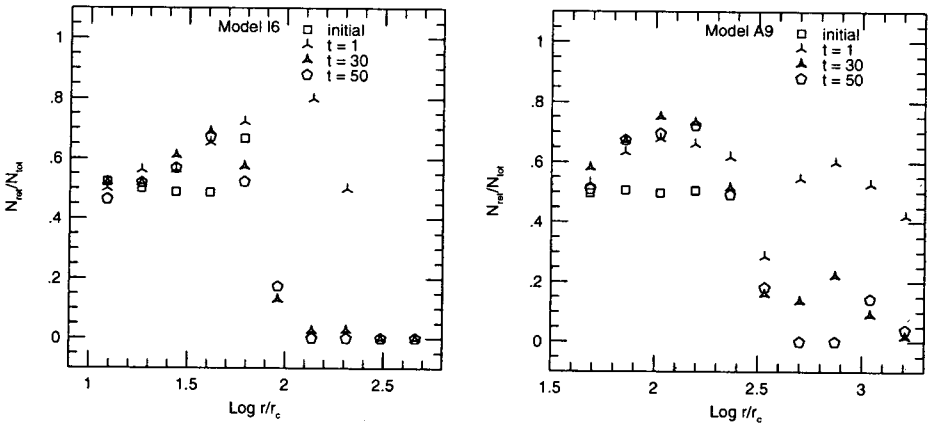

Fig. 6.— The evolution of the fraction of retrograde orbits.

is established during one relaxation time. Then the probability of evaporation during one relaxation time may be set equal to the fraction of stars for which the velocity is greater than twice the rms velocity in a Maxwellian distribution. This simple estimate gives 7.4×10^{-3} for the evaporation rate. Spitzer and Härm (1958) found an escape rate of 8.5×10^{-3} for systems with uniform density and a flat-bottomed potential. The initial mass-loss rate per unit time is correctly given in this case. However, it is unrealistic if the distribution is time dependent. In the case of a tidally limited model, where the ratio of half-mass to tidal radius is $r_h/r_t = 0.145$, self-similar solutions of the Fokker-Plank equation (Hénon 1961) for an isotropic velocity distribution gives an escape rate of 4.5×10^{-2} per relaxation time. The Monte Carlo method with a single mass component (Spitzer & Chevalier 1973) gave an escape rate of 0.015 and 0.05 as r_h/r_t was varied from 0.11 to 0.34. Our corresponding values are shown in Table 5a and 5b. The escape rates per relaxation time are given at several orbital time. We list the case of single mass model for the comparison. Although the escape rates show small time dependence, our results are generally consistent with multi-mass models by Lee & Goodman (1995) and Giersz & Heggie (1997).

All the models show more escapers in multi-mass cases than in single-mass cases. This is because there are more mass in outer region in multi-mass case (Fig. 7), which receives more tidal force than in single-mass cases. Although single-mass models experience more diffusion process, the tidal effect gives more influence on the escaping rates. In the diffusion only Model A2 there are more stars piled up just outside the cutoff radius seen in Figure 4b. The amount of diffusion in single-mass case is bigger, but the escape rate is smaller than that in multi-mass case (Model I2 & A2 in Table 5a & 5b), which seems to be controversial. This can be explained by following. There are less diffusion processes in multi-mass case, but the amount of diffusion imposed to low mass stars are bigger than the average diffusion process and they can be kicked out further to become escapers. These effects are less significant in isotropic case (Model I2) than in anisotropic case (Model A2) because the difference of mass concentration is smaller in isotropic case as seen in Figure 7. When both the tide and diffusion process are imposed, they can be added and give more escape rates in multi-mass cases. And there are more escapers in isotropic multi-mass models than in anisotropic multi-mass models, because the distribution of stars in each mass component of isotropic case is spread wide in energy and angular momentum space, which can escape easily, whereas the higher mass component of anisotropic case concentrates in lower angular momentum.

(g) The Evolution of the Mass Function

The short relaxation time in globular clusters leads to the mass segregation, which makes the heavy stars be more in central region and the light stars in outer region. And the tidal force is more effective in the outer region. Because the low mass stars can escape easily, a flattening of the IMF is expected as a result of the dynamical evolution (Lee *et al.* 1991; Vesperini & Heggie 1997). The strength of the tide on the star is independent of the mass of the star, although the diffusion process is more effective on the low mass stars. It turns out the diffusion coefficient for low mass stars is not much larger than that for the high mass stars in our models. So the escape of stars with the Galactic tide does not depend much on their masses a lot. The previous works usually focus on the mass function inside the globular clusters. But our results can explore the features of the mass function beyond the tidal radii because of our moderate criterion of escape radius ($\sim 10r_c$).

Table 5a. Escape rates in single-mass models

Model	t/τ_o			
	10	20	30	50
I2	7.677×10^{-3}	6.428×10^{-4}	1.934×10^{-3}	0
I3	1.271×10^{-2}	6.803×10^{-3}	5.489×10^{-3}	6.940×10^{-4}
I4	2.261×10^{-1}	2.136×10^{-1}	1.768×10^{-1}	1.064×10^{-1}
I5	2.640×10^{-3}	2.999×10^{-3}	2.688×10^{-3}	2.731×10^{-3}
I6	7.815×10^{-2}	9.278×10^{-2}	8.792×10^{-2}	6.741×10^{-2}
A2	6.152×10^{-5}	1.029×10^{-5}	1.031×10^{-5}	0
A4	1.244×10^{-4}	4.185×10^{-5}	7.355×10^{-5}	0
A6	1.085×10^{-2}	6.776×10^{-3}	5.465×10^{-3}	5.482×10^{-3}
A7	3.153×10^{-4}	3.706×10^{-4}	1.066×10^{-4}	2.151×10^{-4}
A9	9.448×10^{-3}	9.039×10^{-3}	7.894×10^{-3}	7.107×10^{-3}

Table 5b. Escape rates in multi-mass models

Model	t/τ_o			
	10	20	30	50
I2	5.178×10^{-3}	2.477×10^{-3}	2.990×10^{-3}	3.400×10^{-3}
I3	5.227×10^{-2}	1.815×10^{-2}	1.227×10^{-2}	3.867×10^{-3}
I4	3.442×10^{-1}	3.659×10^{-1}	3.105×10^{-1}	1.640×10^{-1}
I5	6.841×10^{-3}	7.005×10^{-3}	8.954×10^{-3}	5.339×10^{-3}
I6	1.128×10^{-1}	1.631×10^{-1}	1.556×10^{-1}	8.781×10^{-2}
A2	5.200×10^{-3}	7.277×10^{-3}	7.192×10^{-3}	4.315×10^{-3}
A4	1.531×10^{-2}	3.500×10^{-3}	6.292×10^{-3}	4.314×10^{-3}
A6	9.756×10^{-2}	8.754×10^{-2}	4.884×10^{-2}	5.761×10^{-2}
A7	8.353×10^{-3}	1.056×10^{-2}	1.445×10^{-2}	7.832×10^{-3}
A9	6.057×10^{-2}	7.892×10^{-2}	7.861×10^{-2}	5.551×10^{-2}

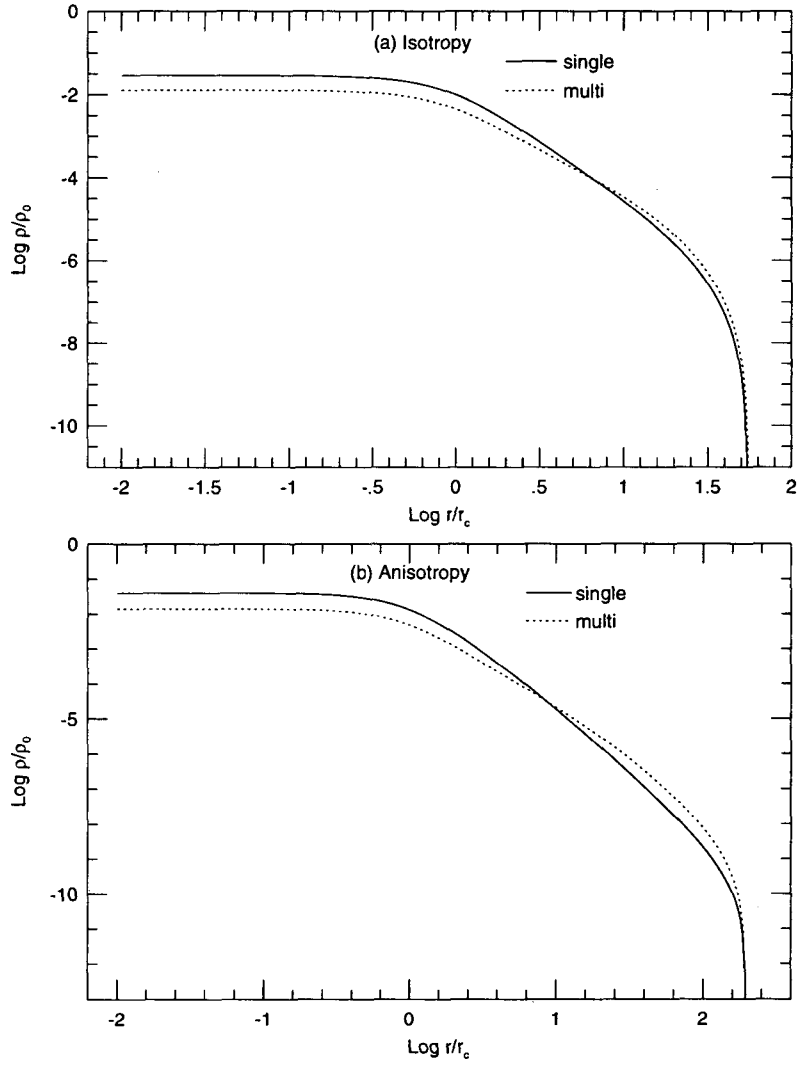

Fig. 7.— Theoretical density plot for single-mass model and multi-mass model.

We define the mass function index difference Δx as

$$\Delta x = \frac{\log n_5 - \log n_4}{\log m_5 - \log m_4} - \frac{\log n_2 - \log n_1}{\log m_2 - \log m_1}, \quad (17)$$

where n_1, n_2, n_4 and n_5 are the number of stars (1 ; highest mass component, 5 ; lowest mass component), and m_1, m_2, m_4 and m_5 are the mass of stars of each mass class. If Δx increases, mass function departs from power law, and the fraction of low mass stars is getting high. The models (Model I2, I3, I5, A2, A4 & A7) with the tidal effect only or the diffusion process only have little number of escapers, which causes large statistical fluctuations. So Δxs' of models with both the tide and the diffusion in three regions of the globular clusters are shown in Figure 8a and 8b for isotropic and anisotropic cases respectively. Although the initial data are generated from power law, Δx inside the cluster is not zero because we use the data outside the critical radius where the effect of mass segregation appears. The Δxs' in anisotropic models are getting smaller than the initial values inside the cutoff radius, but almost same in isotropic models. This flattening in mass function is because the distribution of high mass stars in anisotropic models is in low angular momentum region comparing with that of low mass stars (Fig. 9), therefore low mass stars are easily removed. As a result, Δxs' for the escapers in isotropic models are very similar to the values of the region between critical radius and cutoff radius, whereas they are a little bit larger in anisotropic models. The small flattening effect seems to be contradictory to other results (Lee, Fahlman & Richer 1991 ; Vesperini & Heggie 1997) because there is not constant supply of stars inside the critical radius in our scheme of hybrid method. Nevertheless the qualitative result can be obtained beyond the critical radius.

In isotropic models, high mass stars are relatively more concentrated in the region of low energy and high angular momentum (Fig. 9 (1)) where the diffusion process is more efficient, so high mass stars can be kicked further than low mass stars. And this gradient of distribution beyond cutoff radius will be enforced when stronger tidal effect is imposed like in circular orbit. Therefore the fraction of high mass stars between cutoff radius and five times of cutoff radius is smaller in Model I4 (case of circular orbit) that in Model I6 (case of eccentric orbit), but it is opposite in the region between five times of cutoff radius and ten times of cutoff radius (Fig. 8a (b) & (c)). The distribution of low mass stars in energy-angular momentum space for anisotropic models is wider than that of high mass stars, whereas most of high mass stars have low angular momentum (Fig. 9 (2)), so spatial distribution of low mass stars are more extended by stronger tidal force. So the ratio of low mass stars in Model A6 (case of circular orbit) is higher beyond cutoff radius than that in Model A9 (case of eccentric orbit). But this difference is getting smaller beyond five times of cutoff radius due to steady supply from diffusion process. And Δxs' are bigger than those inside the cutoff radius (Fig. 8b)

VI. SUMMARY

In this paper, we present numerical simulations of the tidal evolution of multi-mass component globular clusters under the influence of internal diffusion and the Galactic tide. This is the extension of our previous work (Paper I and Paper II) where single-mass models are simulated. So we focus on the differences between single-mass models and multi-mass models and the evolution of the mass function in this paper.

First the general evolution in multi-mass models is similar to single-mass models, although there are several differences. There is no evidence for dependence on the orbital phase of the cluster as in Paper I and Paper II.

The Galactic tidal effects are more effective in outer part of the clusters, so there are more escaping process in multi-mass case which has more mass in the outer region than single-mass case has. But the diffusion process is more effective in more concentrated mass distribution, then more stars are likely to kicked out from the center in the case of single-mass models. However the net escapers in the diffusion case of multi-mass models are bigger due to larger diffusion coefficient of low mass stars which are the primary escapers. Therefore the Galactic tide and the diffusion process can accelerate the escaping rates in multi-mass models. The mass-function evolutions show that the fraction of low mass stars beyond the cutoff radius in anisotropic models with the tide and diffusion is larger than that in isotropic models.

ACKNOWLEDGEMENTS

The authors wish to acknowledge the financial support of the Korea Research Foundation made in the program year of 1997. We thank the referee for helpful comments that improved this work. We also thank D. N. C. Lin for a useful formulation of mass-function analysis and a careful reading of the manuscript.

REFERENCES

Aarseth, S. J. 1985, in Multiple Time Scales, ed. J. W. Brackhill and B. I. Cohen (New York: Academic), p. 377

Allen, A. J., & Richstone, D. O. 1988, ApJ, 325, 583

Aguilar, L. A., Hut, P., & Ostriker, J. P. 1988, ApJ, 335, 720

Aguilar, L. A., & White, S. D. M. 1985, ApJ, 295, 374

Capaccioli, M., Ortolani, S., & Piotto G. 1991, A&A, 244, 298

Capaccioli, M., Piotto G.,& Stiavelli, M. 1993, MNRAS, 261, 819

Fall, S. M., & Rees, M. J. 1977, MNRAS, 181, 37p

Giersz, M., & Heggie, D. C. 1996, MNRAS, 279, 1037

Giersz, M., & Heggie, D. C. 1997, MNRAS, 286, 709

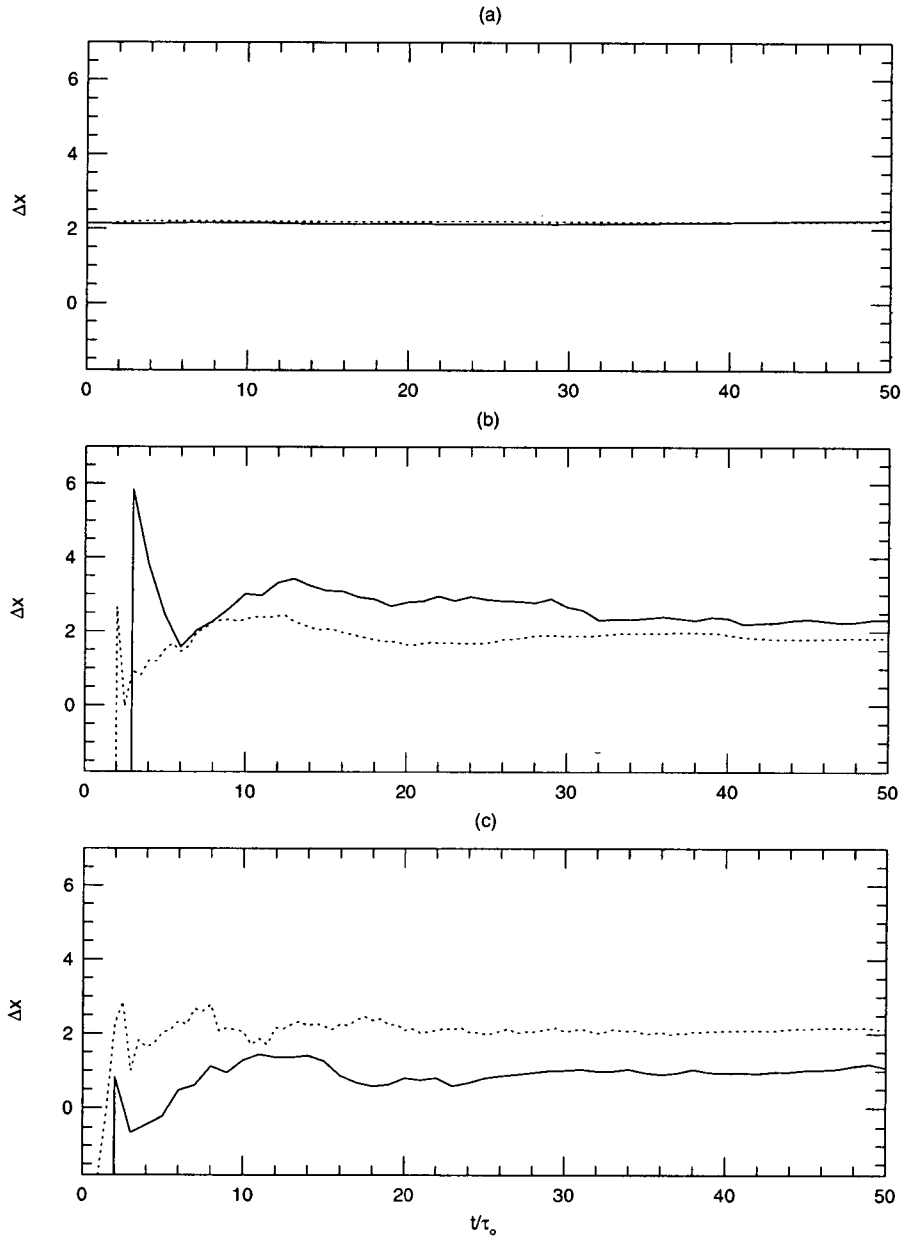

Fig. 8(a).— The time evolution of Δx in isotropic models of I4 and I6, respectively, with solid and dotted lines. The region in (a) is between the critical radius and cutoff radius. The region between the cutoff radius and five times of cutoff radius is in (b). And the region in (c) is between five and ten times of cutoff radius.

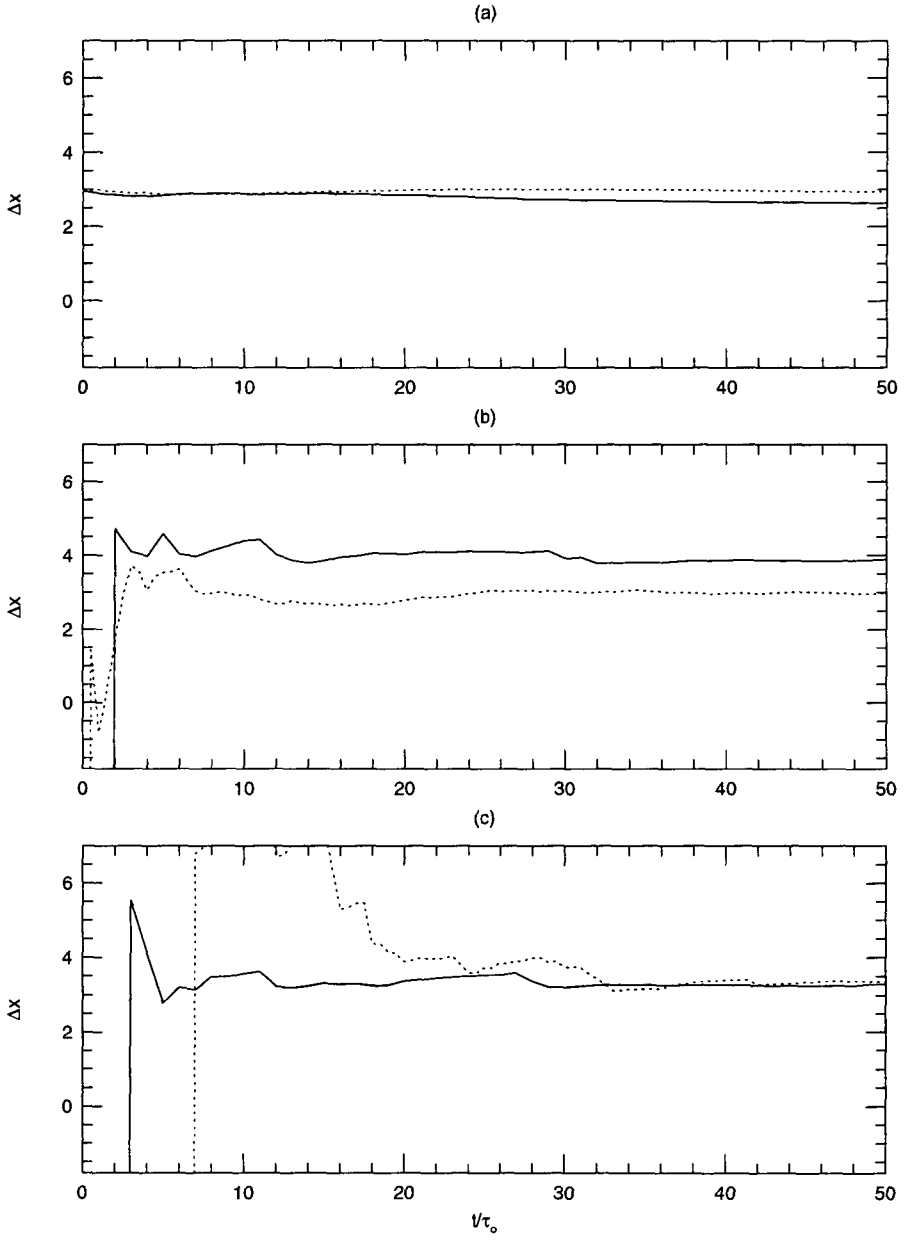

Fig. 8(b).— The time evolution of Δx in anisotropic models of A6 and A9, respectively, with solid and dotted lines. The region in (a), (b) and (c) are same as in Fig. 8(a).

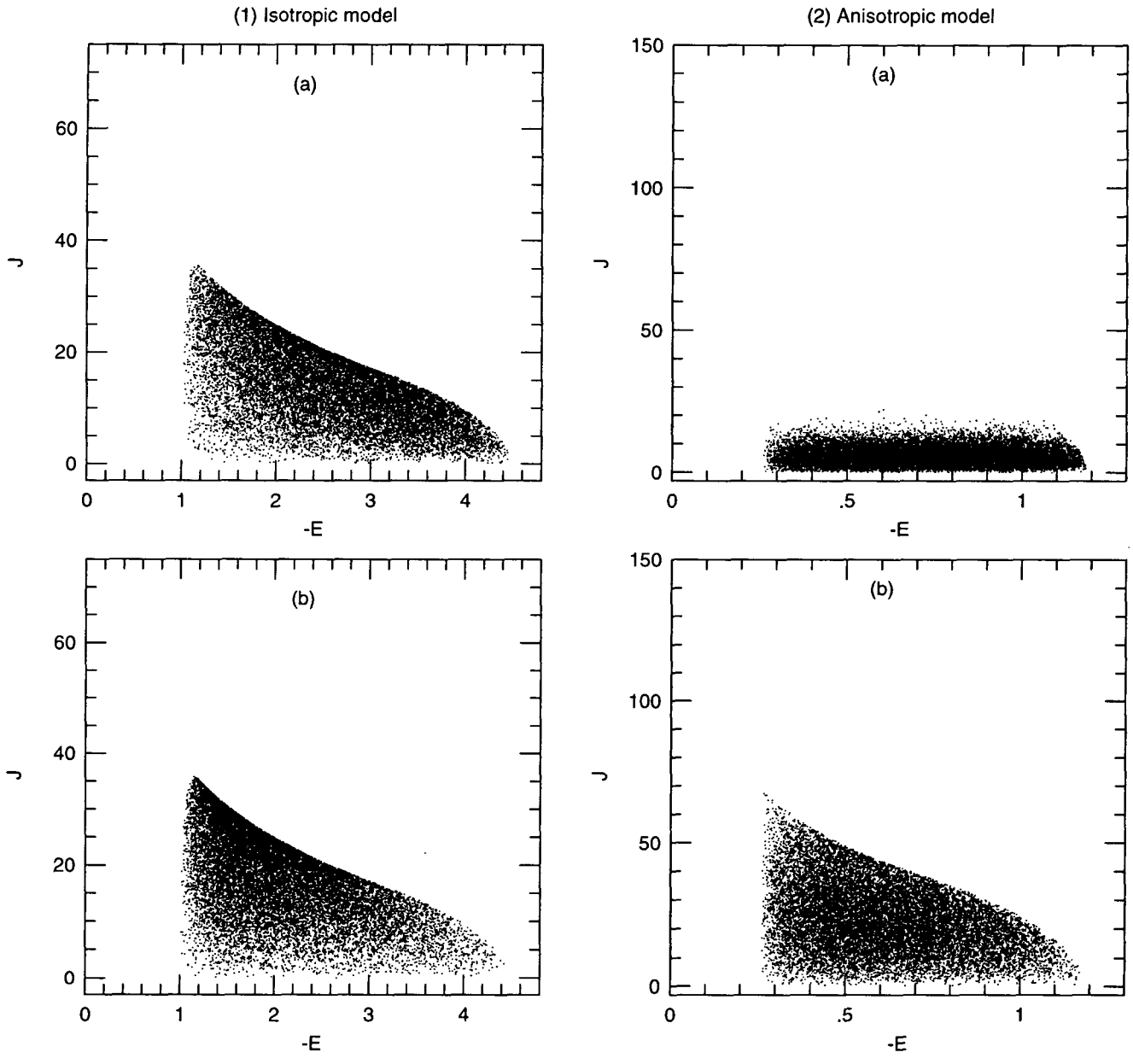

Fig. 9.— Energy and angular momentum distribution for isotropic models and anisotropic models. The number of high mass stars in (a) is same as that of low mass stars in (b) to enforce the distribution.

Gunn, J. E., & Griffin, R. F. 1979, AJ, 84, 752

Illingworth, G., & Illingworth, W., 1976, ApJ, Suppl.,30, 227

Innanen, K. A. 1979, AJ, 84, 960

King, I. R. 1962, AJ, 67, 471

———. 1966, ibid., 71, 64

Lee, H. M., Fahlman, G. G., & Richer, H. B. 1991, ApJ, 366, 455

Lee, H. M., & Goodman, J. 1995, ApJ, 443, 109

McClure, R. D. et al. 1986, ApJ, 307, L49

Oh, K. S., & Lin, D. N. C. 1992, ApJ, 386, 519 (Paper II)

Oh, K. S., Lin, D. N. C., & Aarseth, S. J. 1992, ApJ, 386, 506 (Paper I)

Ostriker, J. P., Binney, J., & P. Saha 1989, MNRAS, 241, 849

Ostriker, J. P., Spitzer, L., & Chevalier, R. A. 1972, ApJ, 176, L51

Peterson, C. J., & King, I. 1975, AJ, 80, 427

Piotto G. 1991, in Janes K., ed., ASP CONF. SER. 13, Formation and Evolution of Star Clusters, ASP, San Francisco, p. 200

Richer, H. B., Fahlman, G. G., Buonanno, R., & Fusi Pecci, F. 1990, ApJ, 359, L11

Ross, D. J., Mennim, A., & Heggie, D. C. 1997, MNRAS, 284, 811

Seitzer, P. 1985, in IAU Symposium 113, Dynamics of Globular Clusters, eds. J. Goodman and P. Hut, (Dordrecht: Reidel), 343

Shapiro, S. L., & Marchant, A. B. 1978, ApJ, 225, 603

Spitzer, L. 1962, in Physics of Fully Ionized Gases, (2nd ed. ; New York : Interscience Publishers), §§5.2 and 5.3

Spitzer, L., & Chevalier, R. A. 1973, ApJ, 183, 565

Spitzer, L., & Hart, M. H. 1971, ApJ, 164, 399

Spitzer, L., & Shapiro, S. L. 1972, ApJ, 173, 529

Spitzer, L., & Shull, J. M. 1975, ApJ, 201, 773

Spitzer, L., & Thuan, T. X. 1972, ApJ, 175, 31

Vesperini, E., & Heggie, D. C. 1997, MNRAS, 289, 898

Webbink, R. F. 1985, in IAU Symposium 113, Dynamics of Star Clusters, ed. J. Goodman and P. Hut (Dordrecht : Reidel), 541